Chemical Engineering Journal 162 (2010) 844–851

Contents lists available at ScienceDirect

Chemical Engineering Journal

journal homepage: www.elsevier.com/locate/cej

Microfluidic synthesis of amorphous cefuroxime axetil nanoparticles with size-dependent and enhanced dissolution rate

Jie-Xin Wang[a,*], Qian-Xia Zhang[a], Yue Zhou[b], Lei Shao[b], Jian-Feng Chen[b,**]

[a] Key Lab for Nanomaterials, Ministry of Education, Beijing University of Chemical Technology, Beijing 100029, PR China
[b] Research Center of the Ministry of Education for High Gravity Engineering and Technology, Beijing University of Chemical Technology, Bei San Huang Dong Road 15, Beijing 100029, PR China

ARTICLE INFO

Article history:
Received 28 January 2010
Received in revised form 13 June 2010
Accepted 17 June 2010

Keywords:
Microfluidics
Cefuroxime axetil (CFA)
Nanoparticles
Dissolution
Nanoprecipitation

ABSTRACT

In this work, size-controllable nanoparticles of amorphous cefuroxime axetil (CFA), a poorly water-soluble drug, have been prepared in a Y-junction microchannel reactor (YMCR) by nanoprecipitation for enhancing dissolution rate of CFA. The effects of the operation parameters, such as flow rate of CFA acetone solution, antisolvent flow rate, overall flow rate, CFA concentration and precipitation temperature, on particle size and size distribution were experimentally investigated. The results indicated that the particle size obviously decreased from 1100 to 630 nm with decreasing the CFA solution flow rate from 16 to 2 mL/min, and decreased from 450 to 350 nm with the decreased temperature from 50 to 5 °C. However, with the increase of the antisolvent flow rate at a fixed CFA solution flow rate of 4 mL/min, the particle size obviously decreased from 1229 nm (20 mL/min) to 581 nm (60 mL/min), and then increased to 698 nm (80 mL/min). Also, the particle size firstly decreased and then increased with the increase of the overall flow rate and CFA solution concentration. The as-prepared CFA nanoparticles displayed a size-dependent and significantly enhanced dissolution property when compared to raw CFA and commercial spray-dried CFA. This work suggests that the continuous synthesis in a microfluidic reactor is a simple and economic way to prepare pharmaceutical nanoparticles with tunable sizes.

1. Introduction

A surprisingly large proportion of new drug candidates emerging from drug discovery programmes is insoluble and therefore poorly bioavailable, leading to abandoned development efforts [1]. The great challenge for the pharmaceutical development is to create new formulas and drug-delivery systems to overcome solubility problems of these drug candidates. Among various strategies to address the solubility issues, reducing the drug particle sizes has emerged as an effective and versatile option [2,3]. Decreasing the size increases the surface area, which results in an increase in the dissolution rate of these drugs in aqueous media such as body fluids [4,5]. Although many techniques for size reduction are available, their applicability is limited because of poor control of particle size, morphology, and scalability in comparison to liquid antisolvent precipitation (LASP) [6–8].

The precipitation of a solid solute is achieved in the LASP process through an increase in the molar volume of solution and, hence, a decrease in the solvent power for the solute by addition of a non-solvent (antisolvent). Two main steps in the process are the mixing of the solution and antisolvent streams to generate supersaturation (the driving force for precipitate formation) and the precipitation of the particles, corresponding to two time scales, the mixing time (τ_{mix}) and the precipitation or induction time (τ_{precip}) [6,8–10]. The dimensionless Damkohler number (Da) is the ratio of τ_{mix} to τ_{precip}. Under poor mixing conditions (large τ_{mix} and Da; Da > 1), the supersaturation is low, and subsequent nucleation rate may be slow relative to growth, leading to large polydisperse particles. As τ_{mix} is reduced relative to τ_{precip} (Da < 1), the greater supersaturation (more rapid nucleation) may lead to a reduction in particle size [6]. Further, this produces rapid and uniform supersaturation in the solution, thereby benefitting the attainment of nanoparticles with narrow size distribution. Hence, it is necessary to decrease τ_{mix} and/or increase τ_{precip} to maintain Da < 1. It is well noted that τ_{mix} can be decreased by employing process intensification technologies, such as microfluidics, high gravity, and ultrasound, etc. [8,11,12].

During the past decade there has been tremendous development in the field of miniaturized fluid-handling systems, known as microfluidic systems [13,14]. The ability of microfluidics to rapidly mix reagents, provide homogeneous reaction environments, continuously vary reaction conditions, and add reagents at precise

* Corresponding author. Tel.: +86 10 64447274; fax: +86 10 64423474.
** Corresponding author. Tel.: +86 10 64446466; fax: +86 10 64434784.
E-mail addresses: wangjx@mail.buct.edu.cn (J.-X. Wang), chenjf@mail.buct.edu.cn (J.-F. Chen).

1385-8947/$ – see front matter © 2010 Elsevier B.V. All rights reserved.
doi:10.1016/j.cej.2010.06.022

time intervals has made it an attractive technology for a myriad of applications [15,16]. Especially, a combination of microfluidics and particle technologies has shown a bright prospect for the development of various inorganic nanoparticles [17–23] and microparticles [24]. However, relatively little research has been done to harness the benefits of microfluidics for the synthesis of organic nanoparticles [25,26], especially drug nanoparticles [11]. This is particularly important in pharmaceutical industry because the preparation of pharmaceutical nanoparticles by bulk mixing usually lacks control of particle size and morphology in the mixing processes, which may compromise the properties of the resulting particles [26]. It is well-known that the particle size and distribution of drug have a great effect on their cellular interactions and biodistribution in body, and making poorly water-soluble drugs into nanoparticles not only increases their dissolution rate but also maximizes their therapeutic effectiveness.

Cefuroxime is a β-lactamase-stable and broad-spectrum cephalosporin. In humans, gastrointestinal absorption of cefuroxime is negligible [27], whereas its 1-acetoxyethyl ester, i.e., cefuroxime axetil (CFA), is an oral prodrug that shows a bioavailability of 30–40% when taken on fasting and 5–60% when taken after food [28]. Commonly, it exists as crystalline and amorphous forms. The amorphous form exhibits a higher bioavailability and adequate stability upon storage [29]. However, like other poorly water-soluble drugs CFA features a low solubility and dissolution rate in the gastrointestinal tract, so its absorption and bioavailability are limited. Presently, micronization of CFA has been achieved mainly using high-gravity technology [7], sono-precipitation technology [30], and supercritical fluid technology [31].

In this work, size-controllable amorphous CFA nanoparticles were synthesized by antisolvent precipitation in a Y-junction microchannel reactor (YMCR). Acetone and isopropyl ether were used as solvent and antisolvent of CFA, respectively. The effects of various process parameters such as the concentration of CFA acetone solution, temperature, the overall flow rate, the flow rate of isopropyl ether and the flow rate of CFA acetone solution on particle size and size distribution were investigated. The commercial CFA and nano-sized CFA were characterized by scanning electronic microscopy (SEM), Fourier transform infrared spectrophotometry (FT-IR), X-ray diffraction (XRD), and differential scanning calorimetry (DSC). The dissolution testing identified the size-dependent and enhanced dissolution rate of the as-prepared CFA nanoparticles.

2. Experimental

2.1. Materials and apparatus

Crystalline CFA raw drug and commercial spray-dried amorphous CFA were both obtained from North China Pharmaceutical Group Beta Co., Ltd. (Hebei, China). Acetone, isopropyl ether (A.R. grade) and sodium dodecyl sulfate (SDS) were supplied by Beijing Chemical Reagent Company (Beijing, China). Deionized water was purified by Hitech-K Flow Water Purification System (Hitech Instrument Co., Ltd., Shanghai, China).

A schematic diagram of the experimental set-up is illustrated in Fig. 1a. The key part is a YMCR (Fig. 1b). The two inlet channels are approximately 400 μm × 500 μm (width × height), and its length is 20 mm. The cross-section of the mixing channel is 800 μm × 500 μm (width × height), and its length is 40 mm (Fig. 1c). The CFA acetone solution and isopropyl ether were introduced into YMCR by a continuous nonpulsatile pump (2PB-80, 0.1–80 mL/min, Beijing Satellite Manufacturing Factory, Beijing, China).

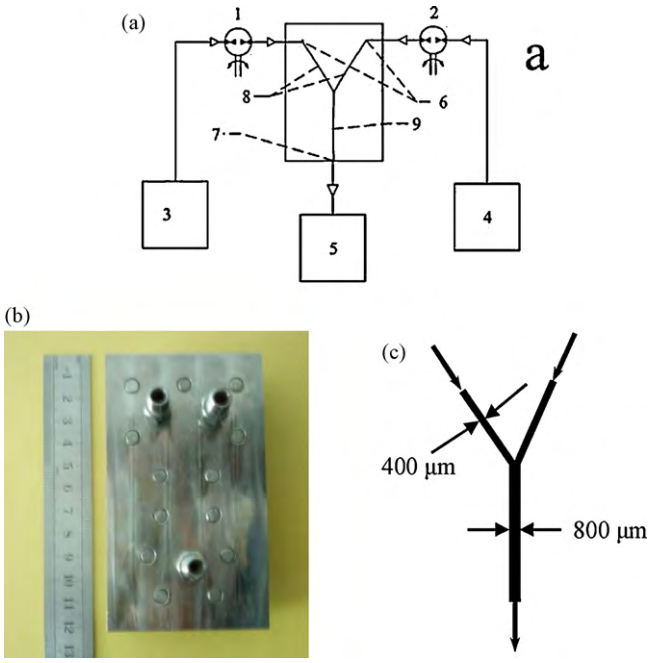

Fig. 1. (a) Schematic diagram of experimental set-up and the structure of the reactor: (1 and 2) continuous nonpulsatile pump; (3 and 4) tank; (5) slurry storage container; (6) inlet; (7) outlet; (8 and 9) microchannels; (b) photograph of YMCR; (c) scheme of YMCR section.

2.2. Preparation of amorphous CFA nanoparticles

Crystalline CFA raw drug was firstly dissolved in acetone and then filtrated through a 0.22 μm nylon membrane to remove impurities. Afterwards, CFA acetone solution as solvent and isopropyl ether as antisolvent were pumped into the two inlet channels, respectively. The rapid mixing of both liquid streams took place at the junction of the two channels (Y-junction) and the precipitation occurred immediately. Subsequently, the suspension obtained from the outlet was diluted with antisolvent for the analysis of particle size and particle size distribution. Finally, the suspension was filtrated through a 0.22 μm nylon membrane and the precipitate was dried at 40 °C under vacuum condition to collect the drug power.

2.3. Characterization

2.3.1. Particle size, morphology and particle size distribution

The morphology and the size of CFA particles were observed using a JSM-6360LV Microscope (JEOL, Japan) at 10 kV after the samples were mounted onto a glass slide fixed on an aluminum cylinder using adhesive tape under vacuum. The particle size and distribution were determined by laser diffractometer (Malvern; ZETASIZER-3000HS).

2.3.2. FT-IR

The molecular states of the raw CFA, commercial CFA and nano-sized CFA were evaluated by a FTIR-8700 Spectrometer (Nicolet, USA) in the range 500–4000 cm^{-1} using a resolution of 4 cm^{-1} and 16 scans. The samples were mixed with KBr powder at 1% (w/w) and pressed into self-supporting disks.

2.3.3. XRD

XRD analysis was performed using a XRD-6000 X-ray Diffractometer (Shimadzu, Japan) to detect the physical characteristics of the raw CFA, commercial CFA and nano-sized CFA. The measuring

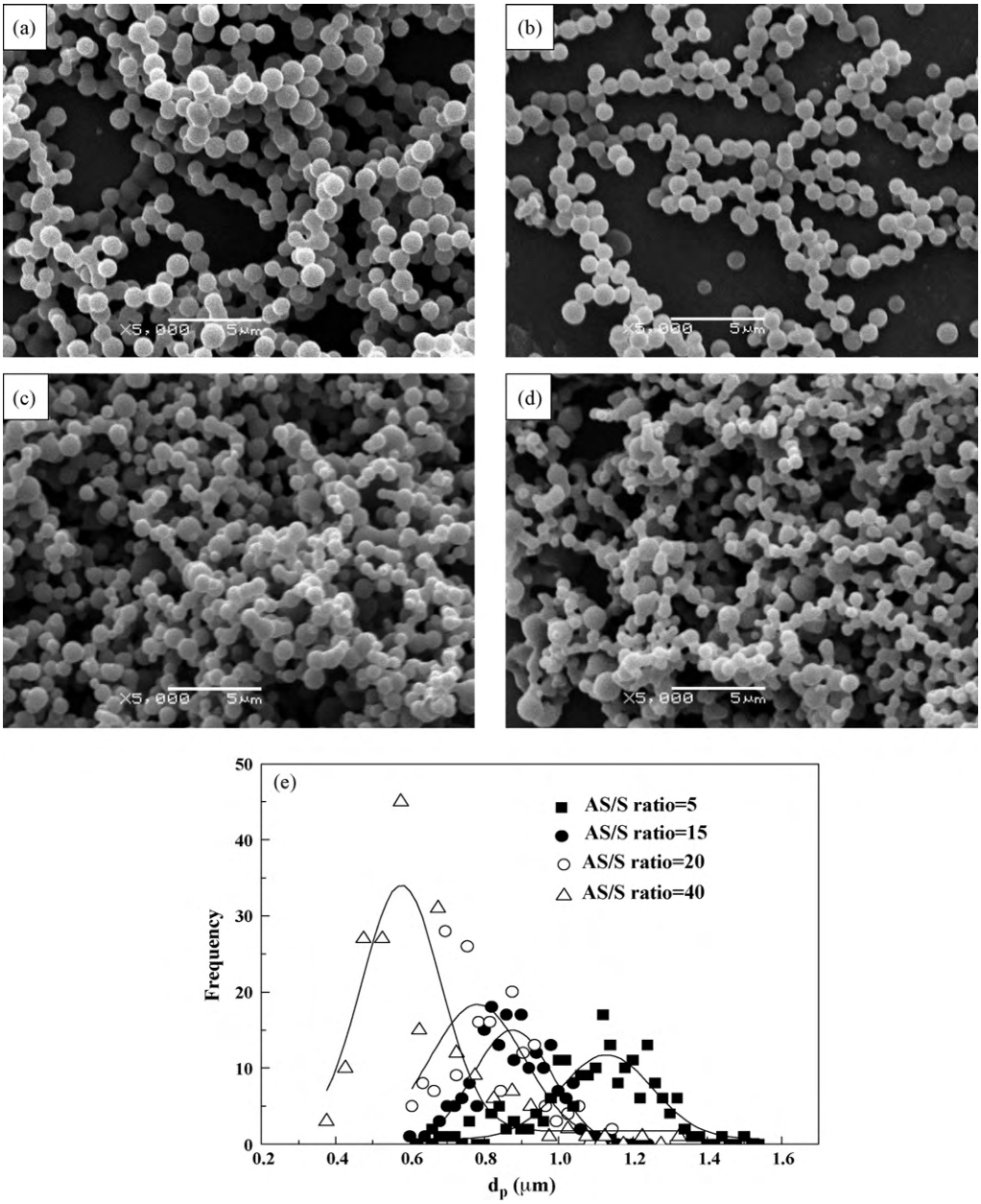

Fig. 2. SEM images of CFA particles prepared at different flow rates of CFA acetone solution: (a) $S = 16$; (b) $S = 5.3$; (c) $S = 4$; (d) $S = 2$; the antisolvent flow rate was set at 80 mL/min. (e) particle size distributions of CFA particles.

unit employed Cu K_α radiation generated at 30 mA and 40 kV. The samples were scanned from 5° to 50° at a step size of 0.05°/min.

2.3.4. DSC

DSC curves of the sample were recorded using a thermal analysis system (Pyris 1, Perkin-Elmer, USA). The sample were placed in an aluminum pan and heated at a rate of 10 °C/min between 30 and 190 °C under a nitrogen atmosphere, which was maintained by nitrogen gas at a flow rate of 25 mL/min. Calibration of the instrument with respect to temperature and enthalpy was achieved using high-purity indium.

2.3.5. Specific surface area

The specific surface areas of raw CFA and ultrafine CFA powder were determined using N_2 adsorption method. Calculation is based on the BET equation. A surface area analyzer (ASAP 2010, Micromeritics, USA) was used. A known amount of powder was loaded into a Quantachrome sample cell and degassed for at least 4 h prior to analysis.

2.3.6. Dissolution testing

Dissolution testing was performed using a dissolution apparatus (D-800LS, Tianjin, China) following the USP Apparatus II (paddle) method. The paddle speed and bath temperature were set at 100 rpm and (37.0 ± 0.5) °C, respectively. The dissolution medium was 0.1 mol/L HCl solution containing 0.1% (w/v) sodium dodecyl sulfate (SDS). Twenty milligrams of drug powder was added into vessels containing 900 mL of the dissolution medium. The samples (5 mL for each) were withdrawn at specific intervals until 90 min and filtered through a 0.22 μm syringe filter.

Afterwards, the concentration of the filtrate was detected by HPLC system. The chromatographic separation was completed using a Waters Sunfire™ C18, reverse-phase column (150 mm × 4.6 mm i.d., 5 μm particle size) protected by a guard

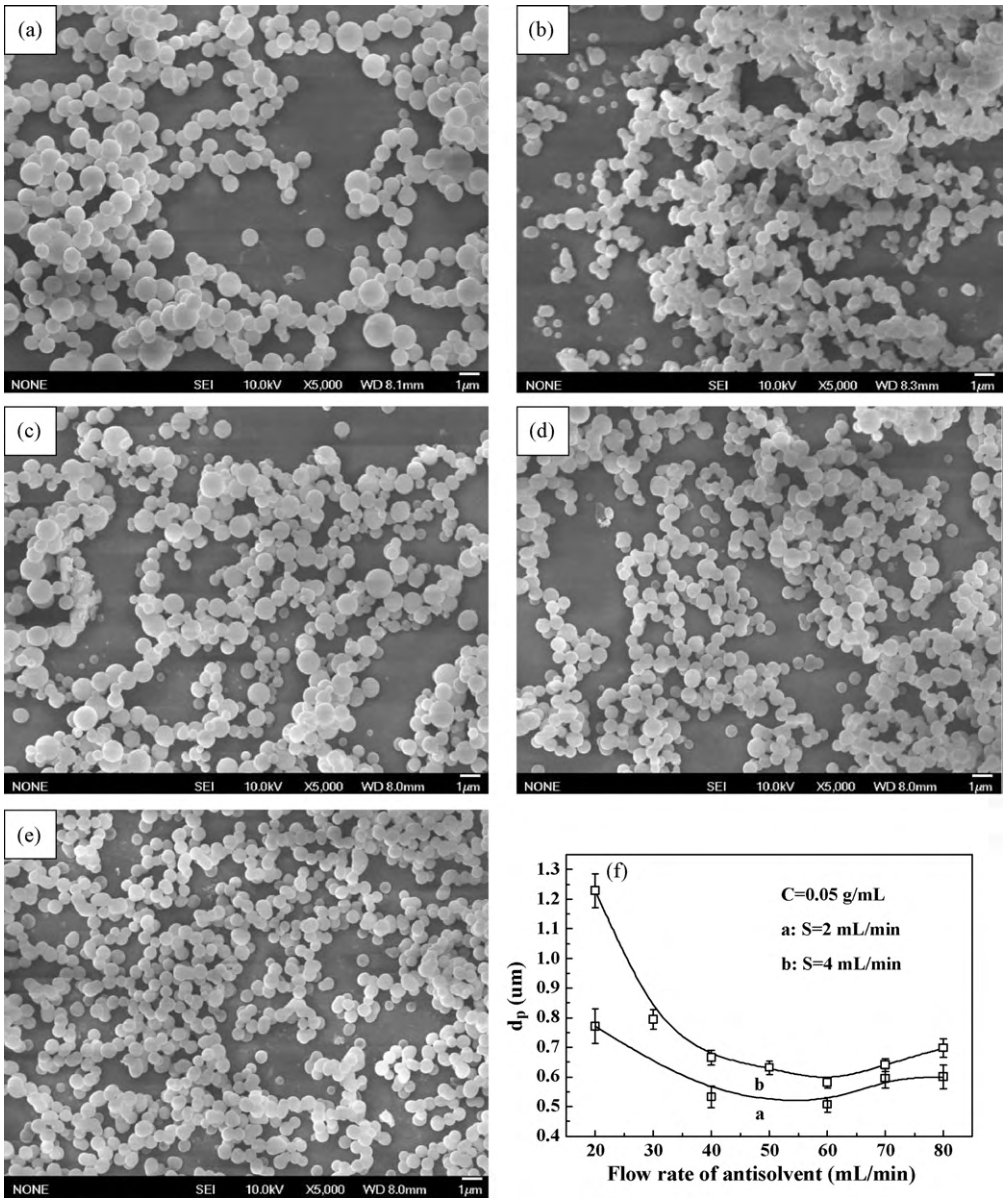

Fig. 3. SEM images of CFA particles prepared at different antisolvent flow rates: (a) 20 mL/min; (b) 40 mL/min; (c) 60 mL/min; (d) 70 mL/min; (e) 80 mL/min. The flow rate of CFA acetone solution was set at 2 mL/min and the concentration of CFA acetone solution was 0.05 g/mL. (f) Effect of the antisolvent flow rate on the average particle size dp.

column (10 mm × 4.6 mm i.d.) which was packed with the same Sunfire™ C18 material. The mobile phase was a mixture of methanol and 0.2 mol/L $NH_4H_2PO_4$ solution (600: 400, v/v). The column was maintained at 25 °C and equilibrated for 40 min with the mobile phase before injection. The injection volume was 50 μL, and the mobile phase was pumped at a flow rate of 1.0 mL/min. The detection wavelength was 278 nm.

3. Results and discussion

3.1. Effect of the flow rate of CFA acetone solution

Fig. 2 shows SEM images of CFA particles prepared at different CFA solution flow rates and the corresponding particle size distributions (PSDs). In this case, the flow rate of antisolvent (AS) was fixed at 80 mL/min. The flow rate of CFA acetone solution as solvent (*S*) was altered to explore its effect on particle size and PSD of CFA particles. It can be clearly seen that the precipitated CFA particles (Fig. 2a–d) were uniform smooth spheres. Besides, a decrease in the flow rate from 16 to 2 mL/min led to an obvious decrease from 1100 to 630 nm in particle size and a narrower PSD (Fig. 2e). This was mainly attributed to the rapid increase of the system supersaturation level as a result of the increase of AS/*S* ratio from 5 to 40.

3.2. Effect of the antisolvent flow rate

Fig. 3 presents SEM images of CFA particles prepared at different antisolvent flow rates and the variation of CFA particle size with increasing antisolvent flow rate at a fixed solvent flow rate. An interesting result could be observed that with the increase of the antisolvent flow rate from 20 to 80 mL/min in the two profiles, the formed CFA particle size quickly decreased up to a flow rate of 50–60 mL/min and then slightly increased. On the one hand, increasing the antisolvent flow rate led to a significant increase of AS/*S* ratio, thereby resulting in a higher supersaturation level. On the other hand, the induced increase of Reynolds number (Re) gave rise to a strong mixing of the solvent with the antisolvent. These

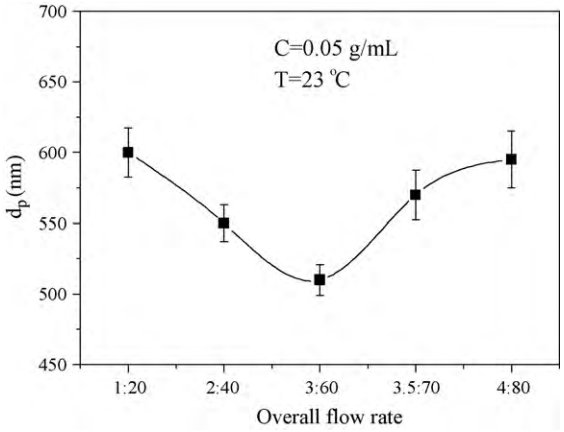

Fig. 4. Effect of the overall flow rate on the average particle size dp.

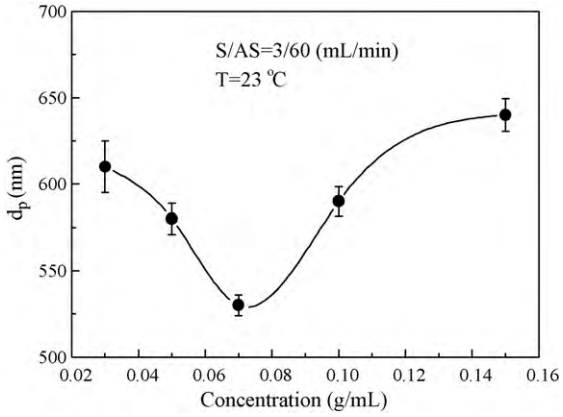

Fig. 5. Effect of CFA concentration on the average particle size dp.

are mainly responsible for the formation of smaller CFA particles with narrower PSD [11,25,32,33]. However, further increasing the antisolvent flow rate from 50–60 to 80 mL/min possibly caused the incomplete mixing of the solvent with the antisolvent (not enough residence time) in the mixing channel of 40 mm length at a higher flow rate so that the solvent diffusion and transfer was not completed [26,34]. In this case, this effect dominated compared with the positive contributions of the increase of the supersaturation and the improvement of micromixing and resulted in a slight increase of CFA particle size. This is similar to the previously reported result on the formation of solid lipid nanoparticles in a microchannel system with a cross-shaped junction [34].

3.3. Effect of overall flow rate

Fig. 4 exhibits the evolution of CFA particle size with the overall flow rate of isopropyl ether and CFA acetone solution at a fixed AS/*S* ratio of 20 (v/v). The particle size and PSD initially decreased with increasing overall flow rate from 21 to 63 mL/min, exhibited a minimum, and increased with further increase in the overall flow from 63 to 84 mL/min. The first size decrease could be explained by an increasing intensity of the mixing between the solvent and the antisolvent with the increasing overall flow rate. In this case, the CFA acetone solution diffused more rapidly into isopropyl ether at a higher flow rate. A uniform spatial concentration distribution was achieved at the molecular scale, and the creation of smaller local supersaturation zones was accelerated, which was beneficial to the formation of smaller particles with narrower PSD. However, when the overall flow rate exceeded 63 mL/min, the particle size increased from 510 to 590 nm, which was in agreement with the result given in Fig. 4. The reason was that the induced incomplete mixing at a higher flow rate resulted in a non-uniform local supersaturation, thereby generating larger particles with wider size distribution. Therefore, the mixing of the solvent and the antisolvent is very crucial to the formation of smaller CFA nanoparticles in a fluidic synthesis. Once a complete mixing or the required residence time is ensured, the increase of flow rate will be beneficial to the preparation of smaller particles.

3.4. Effect of CFA concentration

Fig. 5 displays the variation of particle size with initial CFA concentration in acetone. Clearly, increasing CFA concentration from 0.03 to 0.07 g/mL led to a decrease of the particle size from 610 to 530 nm. This was because an increase in the concentration increased the supersaturation level and the nucleation rate, resulting in a smaller particle size [8]. However, the particle size markedly increased from 530 to 635 nm with further increasing concentration from 0.07 to 0.1 g/mL. This phenomenon might be explained by considering two factors: the number of nuclei formed in the solvent/antisolvent solution and the influence of concentration on the viscosity. At a higher concentration, a large number of nuclei formed in the solvent/antisolvent solution led to particle aggregate and thus formed larger nanoparticles. Besides, the viscosity of CFA solution increased with the increasing concentration, which hindered the diffusion between solution and antisolvent and thus resulted in non-uniform supersaturation and larger particles with broader PSD [35]. Therefore, it can be concluded that the supersaturation level plays an important role in the formation of nanoparticles at a lower concentration, whereas the aggregation and viscosity exert more significant influence on the formation of nanoparticles with the increase of the concentration. The same phenomenon was also observed by other researchers [36].

3.5. Effect of temperature on particle size

Fig. 6 shows the effect of reaction temperature on particle size. It can be found that the particle size decreased from 450 to 350 nm with a decreasing temperature from 50 to 5 °C. This suggested the lower the precipitation temperature, the smaller the particles. The following reasons might be responsible for this. Firstly, the drug solubility decreased with decreasing temperature, and the metastability zone became narrow. Accordingly, it was easy to reach a high supersaturation after the mixing of the solvent and the antisolvent. Secondly, the free energy and heat release decreased in the nucleation process, which favored the formation of the high nucleation rate at a lower temperature. Thirdly, a lower tempera-

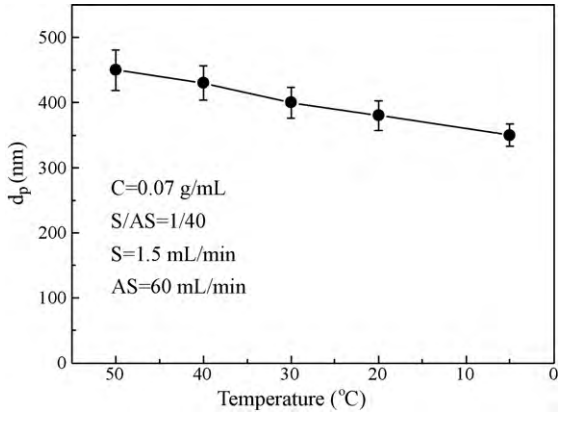

Fig. 6. Effect of the temperature on the average particle size dp.

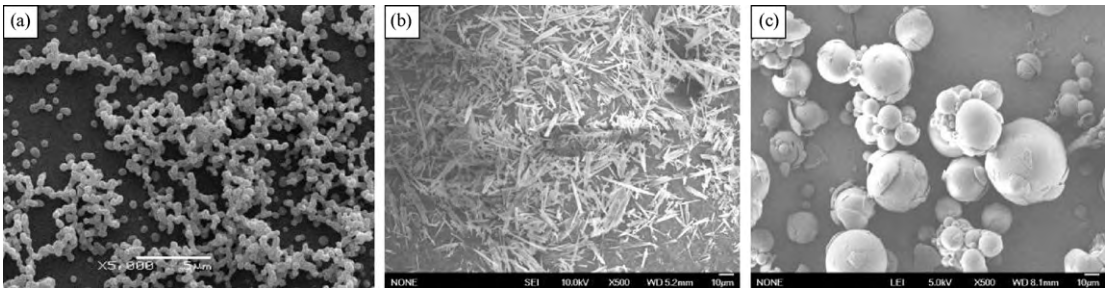

Fig. 7. SEM images of (a) nano-sized CFA, (b) raw CFA and (c) commercial CFA.

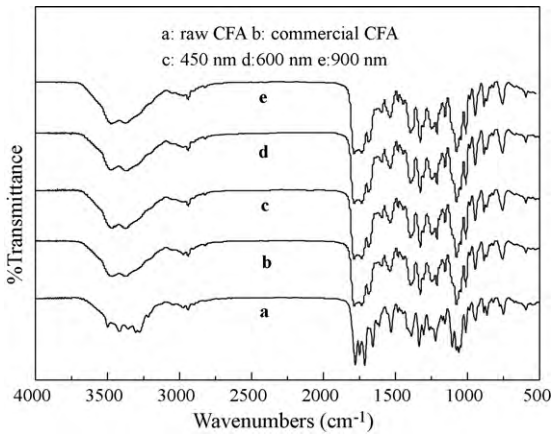

Fig. 8. FT-IR spectra of CFAs: (a) raw CFA, (b) commercial CFA, (c) nano-sized CFA (450 nm), (d) nano-sized CFA (600 nm) and (e) nano-sized CFA (900 nm).

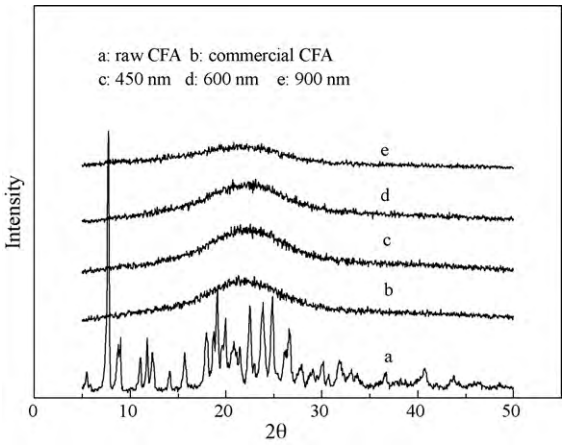

Fig. 9. XRD patterns of (a) raw CFA, (b) nano-sized CFA (450 nm), (c) commercial CFA, (d) nano-sized CFA (600 nm) and (e) nano-sized CFA (900 nm).

ture inhibited the particle growth. Therefore, smaller CFA particles with narrower PSD were obtained at a lower temperature as a result of the high nucleation rate and the low growth rate [35].

3.6. Powder characterization

Since spray drying is the current benchmark technique for generation of amorphous CFA microparticles, the as-prepared nanoparticles were also compared with amorphous CFA obtained by spray drying. Fig. 7 exhibits SEM images of nano-sized CFA, raw CFA and commercial CFA. The raw CFA appeared a rod-like shape with a length of 30–50 μm, whereas the spray-dried commercial CFA product was spherical smooth particles with a broad PSD ranging from 5 to 50 μm. After the precipitation in YMCR, the as-prepared CFA particles had a uniform spherical shape and an average particle size of about 300 nm. It was obvious that the size of CFA nanoparticles was significantly smaller and more uniform than that of raw CFA and commercial CFA. This was beneficial to the increase of the dissolution rate.

Fig. 8 shows FT-IR spectra of raw CFA, commercial CFA and CFA nanoparticles with three sizes in the range of 4000–500 cm^{-1}. The spectra of the CFA were characterized by the NH, NH_2 complex (3480–3210 cm^{-1}), β-lactam (1782 cm^{-1}), acetate (1760 cm^{-1}), 4-ester group (1720 cm^{-1}) and 7-amido (1676 and 1534 cm^{-1}). The identical FT-IR spectra curves of all the CFA samples suggested that there were no chemical changes in the CFA molecular structure caused by the liquid antisolvent precipitation process in YMCR.

Fig. 9 displays XRD patterns of raw CFA, commercial CFA and CFA nanoparticles with two sizes. Raw CFA showed some characteristic high-intensity diffraction peaks, indicating crystalline nature of raw CFA. However, instead of intense crystalline peaks, commercial amorphous CFA and nano-sized CFA produced a halo pattern typical of an amorphous material, where the broad and diffused maxima were caused by a random arrangement of the constituent molecules. This proved that the precipitated CFA power was completely amorphous.

DSC was performed to further investigate the physical state. Fig. 10 presents DSC curves of raw CFA, commercial CFA and CFA nanoparticles with different sizes. The DSC scan of raw CFA showed two sharp melting endothermic peaks at 129 and 181 °C, and the melting enthalpies were 40.196 and 41.812 J/g, proving that raw CFA was not only in crystalline form but also in polymorphs. However, only one endothermic band around 80 °C with lower enthalpy occurred in the DSC scans of commercial spray-dried CFA and nano-sized CFA. Furthermore, the ΔH of 15.143, 21.093, 21.723 and

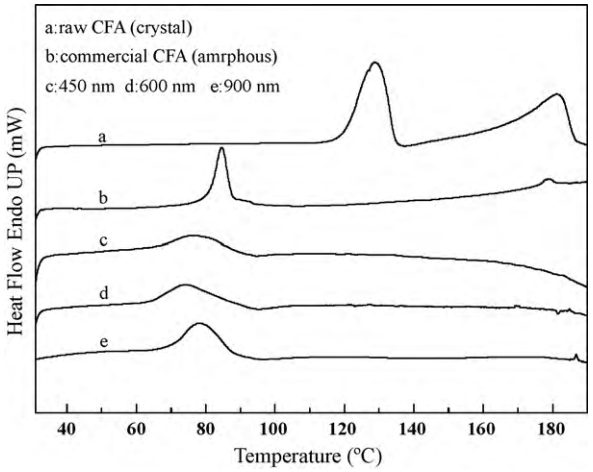

Fig. 10. DSC curves of (a) raw CFA, (b) commercial CFA, (c) nano-sized CFA (450 nm), (d) nano-sized CFA (600 nm) and (e) nano-sized CFA (900 nm).

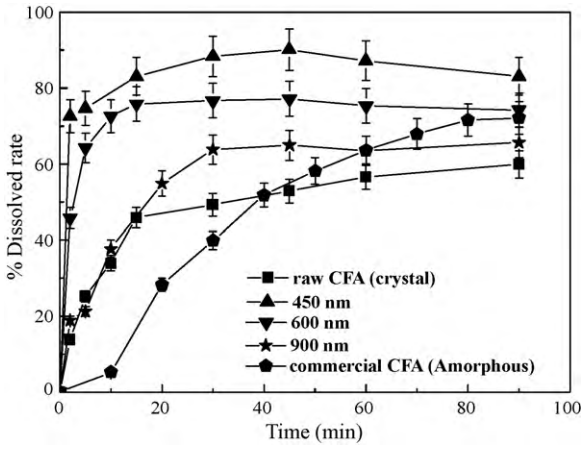

Fig. 11. Dissolution rate profiles of raw CFA, commercial CFA and nano-sized CFA with different sizes.

38.495 J/g of the commercial CFA and nano-sized CFA of 450, 600 and 900 nm were lower than that of the crystalline form. These results indicated that the nano-sized samples and the spray-dried sample were at higher energy state, i.e., amorphous state. This is expected to enhance the dissolution of the water-insoluble drug [3,37,38].

Fig. 11 presents the dissolution profiles of various CFA samples. As expected, compared with raw CFA and commercial CFA, the as-prepared CFA nanoparticles had an obvious burst dissolution in 20 min, as well as a size-dependent and enhanced dissolution rate. During the 90 min testing period, only 57% of raw crystalline CFA and 68% of commercial amorphous CFA dissolved, while about 90% of CFA nanoparticles with an average size of 450 nm was released. The enhanced dissolution of CFA nanoparticles was mainly ascribed to their amorphous structure, uniform small particle size and the higher surface area (1.86 m^2/g for raw CFA versus 8.79 m^2/g for CFA nanoparticles). Furthermore, there was an inverse proportional relationship between the particle size and the dissolution rate. According to the Kelvin equation, as the particle becomes progressively smaller, the surface tension and the molar free energy of product change, thereby resulting in the increased solubility [39]. Besides, It is well-known that the dissolution rate obeys the Nernst–Noyes–Whitney equation, the dissolution rate could be increased by reducing the particle size at the micro- or nano-scale to increase the specific surface area [40,41]. Therefore, as shown in Fig. 11, the dissolution rate of CFA nanoparticles increased with decreasing size, providing an effective route to manipulate the drug dissolution rate.

4. Conclusions

Amorphous CFA drug nanoparticles with narrow PSD, size-dependent and enhanced dissolution rate were prepared in a YMCR. In this process, the CFA particle size and PSD were controlled by adjusting the operation parameters, such as the flow rates of CFA acetone solution and antisolvent, the overall flow rate, the CFA concentration, as well as the temperature. The average drug particle size significantly decreased with the reduction of the flow rate of CFA acetone solution due to the increasing AS/*S* ratio. However, the particle size and PSD firstly decreased and then increased with the increase of antisolvent flow rate, the overall flow rate and the CFA concentration. Lowering the solution temperature was beneficial to the formation of smaller drug particles. The as-prepared CFA nanoparticles exhibited a dramatic improvement in the dissolution rate when compared to raw CFA and commercial CFA. This work suggests that microfluidic preparation of drug nanoparticles by nanoprecipitation may find applications in the newly emerging field of nanomedicine.

Acknowledgements

This work was financially supported by National Natural Science Foundation of China (Nos. 20806004 and 20821004) and National "863" Program of China (Nos. 2009AA033301 and 2007AA030207).

References

[1] B.E. Rabinow, Nanosuspensions in drug delivery, Nat. Rev. Drug Discov. 3 (2004) 785–796.
[2] R.H. Müller, C. Jacobs, O. Kayser, Nanosuspensions as particulate drug formulations in therapy: rationale for development and what we can expect for the future, Adv. Drug Deliv. Rev. 47 (2001) 3–19.
[3] P. Pathak, M.J. Meziani, T. Desai, Y.P. Sun, Nanosizing drug particles in supercritical fluid processing, J. Am. Chem. Soc. 126 (2004) 10842–10843.
[4] G.G. Liversidge, K.C. Cundy, Particle size reduction for improvement of oral bioavailability of hydrophobic drugs: absolute oral bioavailability of nanocrystalline danazol in beagle dogs, Int. J. Pharm. 125 (1995) 91–97.
[5] M. Mosharraf, C. Nystorm, The effect of particle size and shape on the specific dissolution rate of micronized practically insoluble drugs, Int. J. Pharm. 122 (1995) 35–47.
[6] M.E. Matteucci, M.A. Hotze, K.P. Johnston, R.O. Williams III, Drug nanoparticles by antisolvent precipitation: mixing energy versus surfactant stabilization, Langmuir 22 (2006) 8951–8959.
[7] J.F. Chen, J.Y. Zhang, Z.G. Shen, J. Zhong, J. Yun, Preparation and characterization of amorphous cefuroxime axetil drug nanoparticles with novel technology: high-gravity antisolvent precipitation, Ind. Eng. Chem. Res. 45 (2006) 8723–8727.
[8] S.V. Dalvi, R.N. Dave, Controlling particle size of a poorly water-soluble drug using ultrasound and stabilizers in antisolvent precipitation, Ind. Eng. Chem. Res. 48 (2009) 7581–7593.
[9] J. Gradl, H. Schwarzer, F. Schwertfirm, M. Manhart, W. Peukert, Precipitation of nanoparticles in a T-mixer: coupling the particle population with hydrodynamics through direct numerical simulation, Chem. Eng. Process. 45 (2006) 908–916.
[10] B.K. Johnson, R.K. Prud'homme, Flash nanoprecipitation of organic actives and block copolymers using a confined impinging jets mixer, Aust. J. Chem. 56 (2003) 1021–1024.
[11] H. Zhao, J.X. Wang, Q.A. Wang, J.F. Chen, J. Yun, Controlled liquid antisolvent precipitation of hydrophobic pharmaceutical nanoparticles in a microchannel reactor, Ind. Eng. Chem. Res. 46 (2007) 8229–8235.
[12] J.F. Chen, Y.H. Wang, F. Guo, X.M. Wang, C. Zheng, Synthesis of nanoparticles with novel technology: high-gravity reactive precipitation, Ind. Eng. Chem. Res. 39 (2000) 948–954.
[13] K. Jähnishch, V. Hessel, H. Löwe, M. Baerns, Chemistry in microstructured reactors, Angew. Chem. Int. Ed. 43 (2004) 406–446.
[14] H. Pennemann, V. Hessel, H. Löwe, Chemical microprocess technology—from laboratory-scale to production, Chem. Eng. Sci. 59 (2004) 4789–4794.
[15] A.J. deMello, Control and detection of chemical reactions in microfluidic systems, Nature 442 (2006) 394–402.
[16] J. deMello, A. deMello, Microscale reactors: nanoscale products, Lab Chip 4 (2004) 11N–15N.
[17] B.K.H. Yen, N.E. Stott, K.F. Jensen, M.G. Bawendi, A continuous-flow microcapillary reactor for the preparation of a size series of CdSe nanocrystals, Adv. Mater. 15 (2003) 1858–1862.
[18] J.B. Edel, R. Fortt, J.C. deMello, A.J. deMello, Microfluidic routes to the controlled production of nanoparticles, Chem. Commun. 2 (2002) 1136–1137.
[19] J. Wagner, T. Kirner, G. Mayer, J. Albert, J.M. Köhler, Generation of metal nanoparticles in a microchannel reactor, Chem. Eng. J. 101 (2004) 251–260.
[20] X.Z. Lin, A.D. Terepka, H. Yang, Synthesis of silver nanoparticles in a continuous flow tubular microreactor, Nano Lett. 4 (2004) 2227–2232.
[21] M. Takagi, T. Maki, M. Miyahara, K. Mae, Production of titania nanoparticles by using a new microreactor assembled with same axle dual pipe, Chem. Eng. J. 101 (2004) 269–276.
[22] K. Wang, Y.J. Wang, G.G. Chen, G.S. Luo, J.D. Wang, Enhancement of mixing and mass transfer performance with a microstructure minireactor for controllable preparation of $CaCO_3$ nanoparticles, Ind. Eng. Chem. Res. 46 (2007) 6092–6098.
[23] Y. Ying, G.W. Chen, Y.C. Zhao, S.L. Li, Q. Yuan, A high throughput methodology for continuous preparation of monodispersed nanocrystals in microfluidic reactors, Chem. Eng. J. 135 (2008) 209–215.
[24] S. Xu, Z. Nie, M. Seo, P. Lewis, E. Kumacheva, H.A. Stone, P. Garstecki, D.B. Weibel, I. Gitlin, G.M. Whitesides, Generation of monodisperse particles by using microfluidics: control over size, shape, and composition, Angew. Chem. Int. Ed. 44 (2005) 724–728.
[25] S. Zhang, S. Shen, Z. Chen, J. Yun, K. Yao, B. Chen, J. Chen, Preparation of solid lipid nanoparticles in co-flowing microchannels, Chem. Eng. J. 144 (2008) 324–328.
[26] R. Karnik, F. Gu, P. Basto, C. Cannizzaro, L. Dean, W. Kyei-Manu, R. Langer, O.C. Farokhzad, Microfluidic platform for controlled synthesis of polymeric nanoparticles, Nano Lett. 8 (2008) 2906–2912.

[27] G.K. McEvoy, Cephalosporins: cefuroxime sodium and cefuroxime axetil, in: AHFS Drug Information, American Society of Hospital Pharmacists, Inc., Bethesda, MD, 2003, pp. 223–231.
[28] G.K. McEvoy, Cephalosporins: cefuroxime sodium and cefuroxime axetil, in: AHFS Drug Information, American Society of Hospital Pharmacists, Inc., Bethesda, MD, 1994, pp. 152–159.
[29] I. Oszczapowicz, E. Malafiej, M. Szelachowska, A. Horoszewicz-Malafiej, C. Kuklewicz, E. Sieranska, A. Denys, J. Niedworok, Esters of cephalosporins. Part II. Differences in the properties of various forms of the 1-acetoxyethyl ester of cefuroxime, Acta Polon. Pharm. Drug Res. 52 (1995) 397–401.
[30] R.S. Dhumal, S.V. Biradar, S. Yamamura, A.R. Paradkar, P. York, Preparation of amorphous cefuroxime axetil nanoparticles by sonoprecipitation for enhancement of bioavailability, Eur. J. Pharm. Biopharm. 70 (2008) 109–115.
[31] J. Varshosaz, F. Hassanzadeh, M. Mahmoudzadeh, A. Sadeghi, Preparation of cefuroxime axetil nanoparticles by rapid expansion of supercritical fluid technology, Powder Technol. 189 (2009) 97–102.
[32] J.F. Chen, C. Zheng, G.T. Chen, Interaction of macro- and micromixing on particle size distribution in reactive precipitation, Chem. Eng. Sci. 51 (1996) 1957–1966.
[33] K.J. Brian, K.P. Robert, Chemical processing and micromixing in confined impinging jets, AIChE J. 49 (2003) 2264–2282.
[34] S. Zhang, J. Yun, S. Shen, Z. Chen, K. Yao, Formation of solid lipid nanoparticles in a microchannel system with a cross-shaped junction, Chem. Eng. Sci. 63 (2008) 5600–5605.
[35] J.Y. Zhang, Z.G. Shen, J. Zhong, T.T. Hu, J.F. Chen, Z.Q. Ma, J. Yun, Preparation of amorphous cefuroxime axetil nanoparticles by controlled nanoprecipitation method without surfactants, Int. J. Pharm. 323 (2006) 153–160.
[36] U. Bilati, E. Allemann, E. Doelker, Development of a nanoprecipitation method intended for the entrapment of hydrophilic drugs into nanoparticles, Eur. J. Pharm. Sci. 24 (2005) 67–75.
[37] M.S. Kim, S.J. Jin, J.S. Kim, H.J. Park, H.S. Song, R.H.H. Neubert, S.J. Hwang, Preparation, characterization and in vivo evaluation of amorphous atorvastatin calcium nanoparticles using supercritical antisolvent (SAS) process, Eur. J. Pharm. Biopharm. 69 (2008) 454–464.
[38] H.X. Zhang, J.X. Wang, Z.B. Zhang, Y. Le, Z.G. Shen, J.F. Chen, Micronization of atorvastatin calcium by antisolvent precipitation process, Int. J. Pharm. 374 (2009) 106–113.
[39] K.G. Nelson, The Kelvin equation and solubility of small particles, J. Pharm. Sci. 61 (1972) 479–480.
[40] X.S. Li, J.X. Wang, Z.G. Shen, P.Y. Zhang, J.F. Chen, J. Yun, Preparation of uniform prednisolone microcrystals by a controlled microprecipitation method, Int. J. Pharm. 342 (2007) 26–32.
[41] D. Douroumis, A. Fahr, Nano- and micro-particulate formulations of poorly water-soluble drugs by using a novel optimized technique, Eur. J. Pharm. Biopharm. 63 (2006) 173–175.